A Novel Technique for the Measurement of Polarization-Specific Ultrafast Raman Responses

S. Constantine, J. A. Gardecki, Y. Zhou, and L. D. Ziegler*

Department of Chemistry, Boston University, Boston, Massachusetts 02215

Xingdong Ji and Brian Space

Department of Chemistry, University of South Florida, Tampa, Florida 33620

Received: November 22, 2000; In Final Form: June 27, 2001

A simple time domain method for the observation of polarization-specific Raman responses in electronically nonresonant materials is demonstrated. When a cutoff filter is placed in the probe beam path before the detector in the conventional pump−probe configuration, the in-phase dichroic optical heterodyne-detected (OHD) response is enhanced as compared to the usual putative corresponding dichroic response observed when the probe is not dispersed. The ultrafast excited OHD responses of CS_2 obtained by this method are reported for parallel, perpendicular, and magic angle relative orientations of pump and probe pulse polarizations. The observed dispersed dichroic signal can be derived from the real part alone of the third-order nuclear response function. The decay of the CS_2 isotropic response is found to be dominated by a ∼500 fs decay process for times longer than ∼0.7 ps. This relaxation time scale matches the nondiffusive exponential decay seen in the birefringent and dichroic anisotropic responses of CS_2. Calculated instantaneous normal mode (INM) isotropic and anisotropic nuclear response functions are found to exhibit exponential decays in this same 500−600 fs time scale, suggesting that this decay component may be predominantly determined by the distribution of Raman-weighted density of states.

I. Introduction

To fully exploit the capability of Raman measurements to characterize the nature of inter- and intramolecular nuclear degrees of freedom, all unique elements of the molecular transition polarizability tensor should be obtained. For isotropic media, electronically nonresonant Raman cross sections can be completely described by the isotropic and anisotropic components of the polarizability tensor.[1,2] Different scattering mechanisms, selection rules, and relaxation processes can characterize the spectral densities associated with each of these two scattering components.[1−5] During the past decade, the optical heterodyne-detected (OHD) transient birefringence of transparent materials has been shown to be a convenient probe of the low-frequency intermolecular Raman spectral density of liquids due to the impulsive excitation provided by femtosecond pulses.[6−20] In the conventional two-beam OHD configuration, first introduced by Levenson and co-workers,[21] the heterodyning of a phase-controlled portion of the probe pulse itself limits the measurement to observations of the anisotropic or depolarized portion of the Raman scattering tensor.

Previous experimental techniques have been reported for the observation of polarization-specific OHD impulsive Raman measurements. Vohringer and Scherer[22] demonstrated that polarization-specific OHD responses could be observed in a transient grating geometry experiment due to the $\pi/2$ phase heterodyning of the probe scattered in the signal direction from a thermal grating. However, without additional phase-locking pulses, partial or incomplete heterodyning of the third-order response of the sample may be obtained due to this source of local oscillator. Simon and co-workers[23,24] employed a relatively simple two-beam ultrafast technique for the observation of isotropic and anisotropic responses of liquids called position-sensitive Kerr lens spectroscopy (PSKLS). PSKLS is due to the effects of beam distortion on the probe in the far field, resulting from the nonlinear index of the sample. The signal-to-noise ratios of these reported responses, even after long data acquisition times, were still relatively poor compared with standard OHD responses. Subsequent techniques, employing three beams with various schemes to achieve phase-locking of the local oscillator field have been demonstrated. Matsuo and Tahara[25] used a three-pulse, active phase-locking scheme in order to obtain polarization-specific responses. Aside from the added experimental complexity of this method, the relative intensities of different polarization conditions are difficult to compare due to the polarization dependence of the transmittance/reflectivity of optical elements. Most recently, Tokmakoff and co-workers[26] have demonstrated a polarization-specific OHD method that employs diffractive optic beam splitters, to generate a passively stabilized local oscillator field for the observation of phase and polarization-specific, impulsive Raman responses. At the expense of a more complicated experimental setup than the standard OHD impulsive pump−probe arrangement, this configuration provides a measure of polarization-specific third-order responses. Subsequently, Tokmakoff and co-workers[27] have reported polarization-specific Raman responses of liquids obtained by essentially a variation of PSKLS. We have discussed[28] how these simple two beam measurements are related to the so-called Z-scan measurements[29−31] and the standard OHD experimental observables.

* Corresponding author. E-mail: lziegler@chem.bu.edu.

10.1021/jp004277x CCC: $20.00
Published on Web 10/04/2001

The technique reported here allows the observation of polarization-specific Raman responses in the conventional pump−probe two-beam configuration when just a single optical element, an optical cutoff filter, is added to the probe beam path. These effects are demonstrated for the ultrafast Raman responses of CS_2, which has been a benchmark material for both polarization-specific experimental and theoretical studies.[8,17−19,23−26,31−37] After approximately 1 ps the anisotropic OHD birefringent response of CS_2 is well fit by exponential decays of ∼1.7 and ∼ 0.5 ps at room temperature, as first noted by McMorrow, Lotshaw, and co-workers.[6,8] Recent OHD studies[38] have reported temperature-dependent biexponential decay character in the anisotropic ultrafast response of a number of organic liquids including CS_2. While the longer time decay component is attributed to rotational diffusion, the origin of the less evident, faster (∼500 fs) exponential decay has not been established.[8,38] Possible dynamical mechanisms for this second decay include pure dephasing, energy relaxation, or motional narrowing. Additionally, such an exponential feature can also arise from an appropriately shaped inhomogeneous distribution of Raman active modes.[6,8,17] The novel polarization technique described here is used to measure the corresponding relaxation times of the ultrafast isotropic response of liquid CS_2. These experimental results are compared with the polarization-specific nuclear response functions determined by instantaneous normal mode (INM) calculation.

II. Theory

a. Dispersed Responses. The dispersed optical heterodyne-detected (OHD) birefringent or dichroic response as a function of time delay between pump and probe pulses, τ, and the selected probe pulse frequency, Δ_D, is given by[39−41]

$$S_{ijkl}(\Delta_D,\tau) = -2\mathrm{Im}[\tilde{E}_i^{*\mathrm{LO}}(\Delta_D)\tilde{P}_{ijkl}^{(3)}(\Delta_D,\tau)] \quad (1)$$

Δ_D is the detuning of the detected probe pulse frequency, ω_D, from the carrier frequency of the probe pulse (Ω), i.e., $\Delta_D = \Omega - \omega_D$. $\tilde{P}_{ijkl}^{(3)}(\Delta_D,\tau)$ is the Fourier transform of the third-order polarization response of the material polarized along the ith direction generated by temporally sequenced pump/probe field interactions with electric vectors along the j, k, l directions. For pump/probe pulses with identical carrier frequencies, this probe-frequency-dependent response is described by

$$\tilde{P}_{ijkl}^{(3)}(\Delta_D,\tau) = (1/\sqrt{2\pi})\int_{-\infty}^{\infty} dt\, \exp(-i\Delta_D t)\hat{E}_j^{\mathrm{pr}}(t-\tau) \times \int_0^{\infty} d\tau_1\, \hat{E}_k^{*\mathrm{pu}}(t-\tau_1)\, \hat{E}_l^{\mathrm{pu}}(t-\tau_1)\, R_{ijkl}^{(3)}(\tau_1) \quad (2)$$

$R_{ijkl}^{(3)}(t)$ is the third-order impulse response function of the material, and $\hat{E}_j^{\alpha}(t)$ is the pulse envelop of the pump or probe (α = pu, pr) fields. The complex quantity, $\tilde{E}_i^{*\mathrm{LO}}(\Delta_D)$ (eq 1), is proportional to the spectrum (Fourier transform) of the probe field, $\tilde{E}_i^{*\mathrm{pr}}(\Delta_D)$:

$$\tilde{E}_i^{*\mathrm{LO}}(\Delta_D) = (1/\sqrt{2\pi})\exp(-i\theta)\int_{-\infty}^{\infty} dt\, \exp(i\Delta_D t)\, \hat{E}_j^{*\mathrm{pr}}(t-\tau) = (1/\sqrt{2\pi})\exp[i(\Delta_D\tau - \theta)]\, \tilde{E}_j^{*\mathrm{pr}}(\Delta_D) \quad (3)$$

Dichroic and birefringent OHD responses are obtained with in-phase ($\theta = 0$) and $\pi/2$ phase shifted local oscillator fields ($\theta = \pi/2$), respectively. In the usual ultrafast OHD investigation of nonresonant materials, changes in the energy of the total, *nondispersed* probe beam as a function of interpulse delay (τ) are reported.[6−20] The corresponding familiar expressions for OHD birefringence and dichroism[10,39] are recovered when eq 1 is integrated over all probe pulse frequencies (Δ_D).[40,41] As expected for electronically nonresonant materials, observed integrated OHD birefringent ($\theta = \pi/2$) responses are generally more than 1 order of magnitude larger than the corresponding OHD dichroic ($\theta = 0$) responses.[12,42−44] Formally, this difference is due to the larger magnitude of the real part as compared to the imaginary part of this third-order nuclear impulse response function. These relative magnitudes may be seen as resulting, respectively, from constructive and destructive interfering CARS and CSRS-like density matrix pathways contributing to this nuclear response function.[12,43−45]

Within a Born−Oppenheimer description of molecular states, the third-order impulse response function, $R_{ijkl}^{(3)}(t)$, which in general is a complex function, may be written as a sum of contributions from electronic and nuclear degrees of freedom: $R_{ijkl}^{(3)} = R_{ijkl}^{(3e)} + R_{ijkl}^{(3n)}$. When the incident frequencies are not coincident with any regions of one- or two-photon electronic absorption, the corresponding nonresonant electronic response can be taken to be instantaneous and proportional to a real constant.[40,41,48] The nuclear response is formally described in terms of the two-time correlation function of the transition polarizability by $R_{ijkl}^{(3n)}(t) = i/h\langle[\alpha_{ij}(t),\alpha_{kl}(0)]\rangle$.[39]

b. Polarization Considerations. In an isotropic medium, there are only three linearly independent susceptibility elements, or response functions, that obey the well-known relationship: $R_{ZZZZ}^{(3)} = R_{ZZYY}^{(3)} + R_{ZYZY}^{(3)} + R_{ZYYZ}^{(3)}$.[46] By Kleinman's symmetry, $R_{ZZYY}^{(3e)} = R_{ZYZY}^{(3e)} = R_{ZYYZ}^{(3e)} = R_{ZZZZ}^{(3e)}/3$ and thus the nonresonant electronic contribution can be described in terms of just a single susceptibility element. When the relative polarization directions of the pump and probe beams have parallel, perpendicular, or magic angle (54.7°) orientations, the corresponding relative magnitudes of the nonresonant electronic responses, $R_{ZZZZ}^{(3e)}$: $R_{ZZYY}^{(3e)}$:$R_{\mathrm{Mag.Ang}}^{(3e)}$, are in the ratio 3:1:$^5/_3$.[47] For nonresonant Raman transitions, only $R_{ZYZY}^{(3n)} = R_{ZYYZ}^{(3n)}$, and hence two polarization observations, e.g., pump/probe parallel polarized and pump/probe perpendicularly polarized, are necessary for the complete characterization of the nonresonant Raman scattering response (time or frequency domain). These responses can be recast in terms of the anisotropic and isotropic contributions to the Raman (nuclear) response by $R_{\mathrm{Aniso}}^{(3)} = (R_{ZZZZ}^{(3)} - R_{ZZYY}^{(3)})/2$ and $R_{\mathrm{Iso}}^{(3)} = (R_{ZZZZ}^{(3)} + 2R_{ZZYY}^{(3)})/3$. This combination of observed responses is generally taken to allow the contribution of orientational motion to be separated from other sources of Raman response relaxation.[10,44] When the relative angle between the linearly polarized pump and probe pulses is set to the so-called magic angle (54.7°), the observed signal is directly proportional to the isotropic response, i.e., $R_{\mathrm{Mag.Ang}}^{(3)} = R_{\mathrm{Iso}}^{(3)}$.

c. Calculated Spectrogram. A calculated dichroic spectrogram, i.e., the OHD dichroic response as a function of both interpulse delay and probe pulse frequency, is shown in Figure 1 due to a pair of transform-limited 45 fs pulses incident on a material with an impulse response function given by

$$R_{ZZYY}^{(3)}(t) = a\delta(t) - \sum_i \rho(\omega_i)\sin\omega_i t - b\exp(-t/\tau_d)(1-\exp(-t/\tau_r)) \quad (4)$$

where $\rho(\omega_i) = \omega_i\exp(-\omega_i/\omega_c)$ and $\omega_c = 20\ \mathrm{cm}^{-1}$, $\tau_d = 1.7$ ps, $\tau_r = 0.15$ ps, $a = 1200$, and $b = 140$. A response function of this form models a typical depolarized *inter*molecular $R_{ZZYY}^{(3)}$ response.[24] The δ function component represents the instantaneous nonresonant electronic response. The intramolecular librational or collision-induced and orientational diffusive

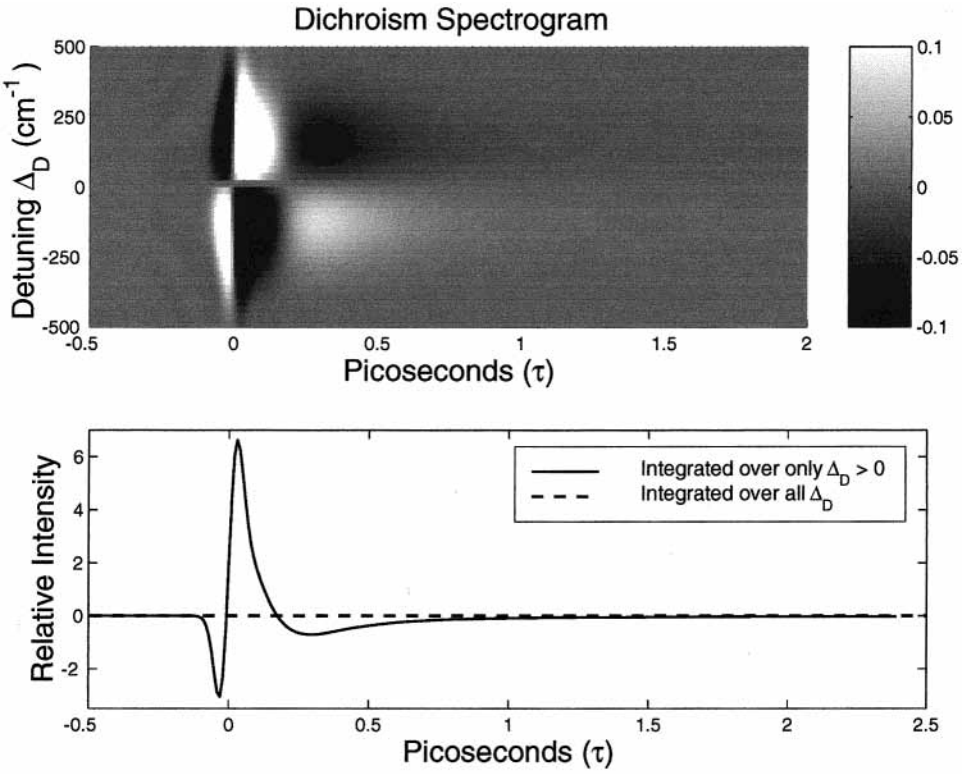

Figure 1. Calculated OHD dichroic spectrogram (upper panel) for an all-real third-order impulse response function due to an instantaneous electronic and intermolecular and diffusive nuclear contributions (see text for more details) and 45 fs pulses. The corresponding OHD signals due to the totally and partially integrated spectrogram are plotted in the lower panel.

nuclear contributions are simulated by the second and third terms, respectively, in eq 4. As seen in Figure 1, which results when eqs 2−4 are substituted in eq 1, a dispersive-like shape with respect to both τ and Δ_D is observed in the region where pump and probe overlap, $\tau \sim 0$. Such a shape characterizes nonresonant electronic dichroic spectrograms.[40,41] In the $\tau < 0$ region, the response is dominated by the instantaneous electronic response. Both electronic and nuclear contributions overlap in the $0 < \tau < \sim 100$ fs region. Antiphased contributions, with respect to the detuning frequency $\Delta_D = 0$, are found at $\tau > \sim 100$ fs due to the intermolecular nuclear responses and exhibit a maximum/minimum at ~300 fs (see Figure 1). When this dichroic OHD spectrogram is integrated over all probe frequencies, the response vanishes, as shown in the lower panel of Figure 1 (dashed line). This is a general result for transform limited pulses when the response function is all real as modeled here (eq 4). This is probably a good approximation for low-frequency, intermolecular modes of interest here.[12,39] However, when the dichroism is observed at a selected frequency, or integrated over only a portion of the probe pulse frequencies, the exact cancellation from the red and blue sides of this dichroic spectrogram is spoiled and a nonzero dichroic response is obtained. The dichroic signal resulting from an integration over the spectrogram responses only on the red side of the probe carrier frequency illustrating this effect is displayed in the lower panel of Figure 1 (solid line). Furthermore, since the dichroic measurement is inherently an in-phase ($\theta = 0$) local oscillator result, there are no polarization restrictions on the relative orientation of the pump and probe beam for this dispersed technique. Thus, nonputative dichroic responses for electronically nonresonant materials may be obtained for *any* relative polarization orientation of pump and probe pulses when the interpulse delay dependence of only a selected portion of the probe pulse spectrum is observed, as demonstrated by the results of the calculations presented in Figure 1. We also briefly note here that convolution of the nuclear impluse response function with the frequency selected nonresonant electronic response yields the corresponding frequency selected Raman response (see Appendix).[56]

III. Experimental Section

The OHD responses are observed in the standard two-beam OKE pump−probe configuration.[6−20] Near transform limited (<1.2 TL) 45 fs pulses centered at 595 nm are used to obtain the data reported here. Ultrafast pulses are produced by an OPA pumped by the second harmonic of a regeneratively amplified Ti:sapphire oscillator operating at 250 kHz. In contrast to the usual experimental observation of nonresonant OHD responses, a low-pass red filter (Schott RG610) is placed in the probe beam just before the detector (photomultiplier tube). This filter has a 50% transmission at 605 nm. Thus, only a portion of the dichroic signal due to third-order polarization components on the red side of the probe carrier frequency contributes to the responses reported here. The use of dispersed OHD dichroic responses for polarization selectivity was first qualitatively demonstrated via monochromator dispersion.[43] However, the use of a low-pass filter for this purpose is simpler and cheaper to implement, avoids potential phase front distortion effects[28] at the monochromator entrance slits, and provides a polarization-independent detection scheme.

Spectroscopic grade CS_2 is used without further purification and flowed through a 1 mm quartz sample cell. The pulses were focused with a 175 mm lens, and pulse energies at the sample were of the order of 10 nJ/pulse. The intensity dependence of these responses was measured in order to ensure that homodyne contamination was minimal (<~5% at signal maximum). Time constants are determined by fits to the observed experimental decays from an initial delay time such that the determined time constants are independent of this choice (typically from $\tau \sim$ 0.7 ps).

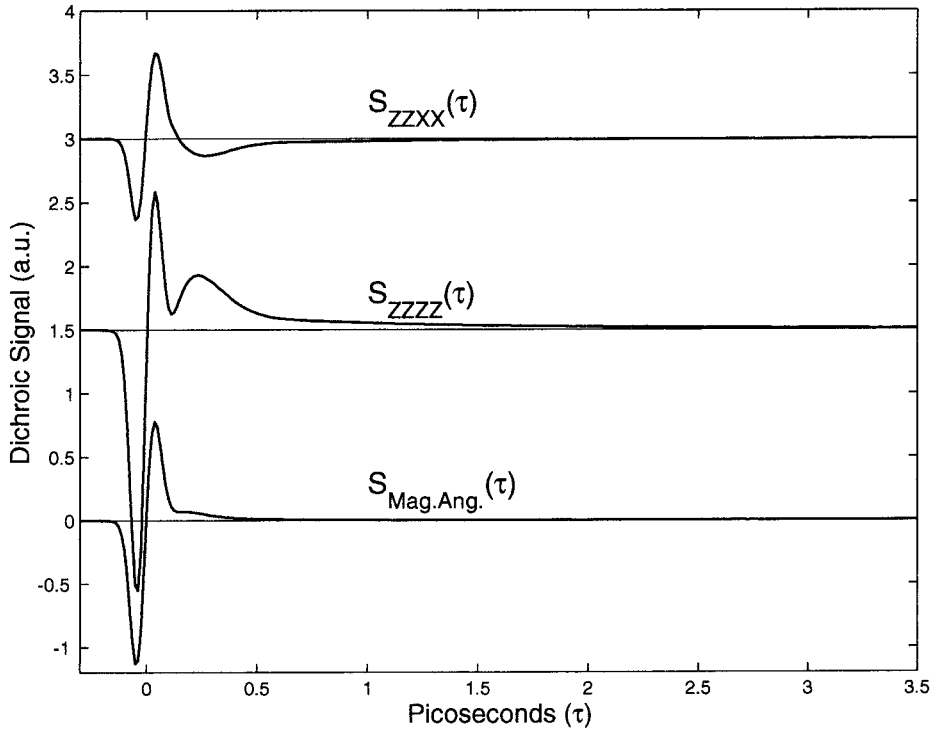

Figure 2. Observed partially integrated, polarization selected OHD dichroic responses of CS_2 obtained with 45 fs pulse excitation centered at 595 nm. A red transmitting filter (RG610) was placed in the probe beam path before the detector. The relative polarization directions of the pump and probe are indicated.

IV. Results and Discussion

a. Polarization-Specific Responses. The partially integrated OHD dichroic CS_2 responses observed for three experimental polarization conditions, parallel, perpendicular, and magic angle pump−probe orientations, are shown in Figure 2. These signals are obtained when a low-pass cutoff filter, which transmits $\lambda > 605$ nm, is placed in the probe beam just before the detector, as described above. The carrier frequency of the 45 fs pulses is ∼595 nm. Unlike the more familiar and previously reported birefringent CS_2 responses,[8,17−19,23−26,33,34] the electronic contribution appears as a dispersive line shape component near $\tau = 0$. Such a response shape is the signature of a frequency-dispersed nonresonant electronic dichroic response.[40] In contrast, the nonresonant electronic response in an OHD birefringent measurement follows the temporal profile of the pulse autocorrelation. The relative intensities of this observed CS_2 electronic component, determined by the depth of the negative going feature at $\tau = -50$ fs, for the parallel, perpendicular, and magic angle pump/probe polarization measurements, are 1.0, 0.31, and 0.55 respectively, in excellent agreement with the values dictated by Kleinman's symmetry.[47] The nuclear portion of the parallel and perpendicular partial integrated dichroic spectrograms, $S^{(3)}_{ZZZZ}$ and $S^{(3)}_{ZZYY}$, have the same relative sign and qualitative shape as the previously reported birefringent observations of these CS_2 responses.[23,25,26]

A test of the self-consistency of the responses acquired by this dichroism technique is demonstrated in Figure 3. The unscaled CS_2 isotropic dichroic response obtained by pump−probe magic angle orientation directly and that determined by $(S^{(3)}_{ZZZZ} + 2S^{(3)}_{ZZYY})/3$ are compared in this figure. As shown here, these two experimental measures of the isotropic scattering response are identical within the precision of these observations.

b. Isotropic and Anisotropic CS_2 Responses. The polarization-specific CS_2 responses shown in Figure 2 clearly display distinctly different decays in the longer time regime ($\tau > 0.5$ ps), as noted in an earlier study.[26] It has been previously reported, and confirmed by measurements in this lab as well, that the birefringent anisotropic response of CS_2 in the $\tau > \sim 0.5$ ps region can be fitted by a sum of two exponentials with decay time constants of ∼0.5 and ∼1.7 ps at room temperature.[8,18] The longer time constant is attributed to the Debye−Stokes−Einstein-like rotational reorientational diffusive relaxation. The log of the anisotropic dichroic response of CS_2 determined by the appropriate linear combination of the observed partially integrated parallel and perpendicularly polarized dichroic responses shown in Figure 2, i.e., $(S^{(3)}_{ZZZZ} - S^{(3)}_{ZZYY})/2$, is plotted in the upper panel of Figure 4. In agreement with the reported analysis of the CS_2 anisotropic response obtained by birefringent observations, the dichroic anisotropic response in the 0.7−6.5 ps region is well fit by a biexponential decay with time constants of 0.52 and 1.65 ps (see Figure 4).

The total many body polarizability is often separated into a portion due to single molecule polarizability contributions and polarizability contributions arising from intermolecular interaction-induced effects.[4,5,37,49] The molecular part, also referred to as the librational contribution, is due to the sum of contributions from polarizability tensors of individual molecules. The interaction (or collision) induced polarizability (CI), usually described in the dipole−induced dipole (DID) approximation, derives from the local field fluctuations at a given scatterer due to induced dipoles of surrounding molecules.

A semilog plot of the isotropic response of CS_2 determined directly by magic angle measurement is shown in the lower panel of Figure 4. The displayed response is the average of two magic angle observations. A fit to a single exponential decay in the 0.7−2.1 ps region corresponding to a decay time of 0.52 ps is also shown in this figure. Thus, while some additional longer time decay components may contribute to this isotropic response, the bulk of the time scale of the decay of this scattering

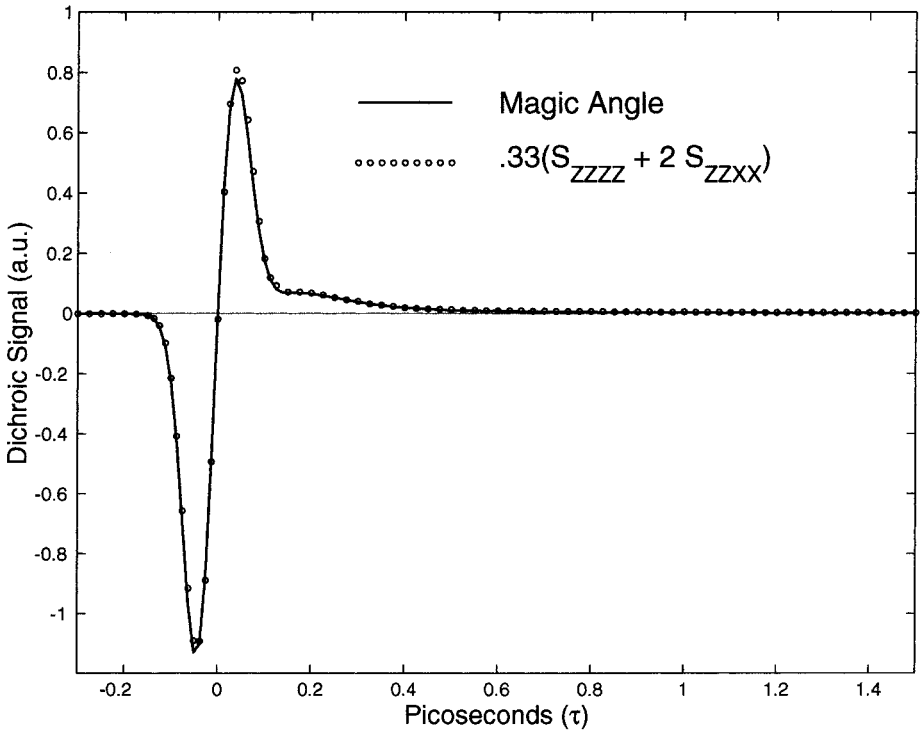

Figure 3. Comparison of the ultrafast CS_2 isotropic response obtained by the magic angle measurement and by the linear combination of the S_{ZZZZ} and S_{ZZXX} measurements.

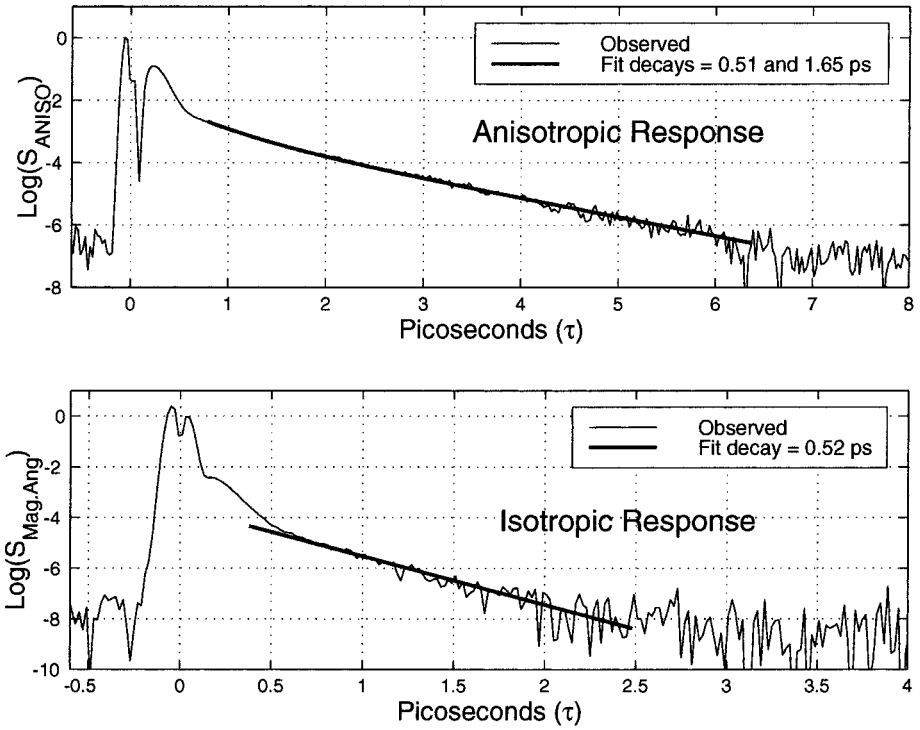

Figure 4. Anisotropic response of CS_2 constructed from the partially integrated dichroic ($S_{ZZZZ} - S_{ZZXX}$) combination is displayed in the upper panel. The results of a double-exponential fit in the 0.7−6.5 ps region is also given. The isotropic response of CS_2 determined by magic angle observation is shown in the lower panel. A fit to an exponential decay in the 0.7−2.4 ps region is also displayed. Note the time scale axis difference for these two plots.

tensor closely matches the shorter time component seen in the anisotropic scattering responses (∼0.5 ps). Fourier analysis reveals some weak contributions from the strongly polarized 660 cm^{-1} intramolecular mode of CS_2 in the partially integrated isotropic response excited by 45 fs pulses and is evident (by Fourier analysis) at longer times. In addition, incomplete suppression of the anisotropic response or, more interestingly, contributions of the rotational diffusion response, first noted by Tokmakoff and co-workers,[48] may also contribute weakly to this isotropic response (see Figure 4). Such contributions to the isotropic response may arise from interaction or so-called collision-induced (DID for example) Raman effects directly[49−51] or via single molecule-CI cross terms for nonrigid molecules.[5] The dominance of this 0.5 ps decay to the CS_2 isotropic response

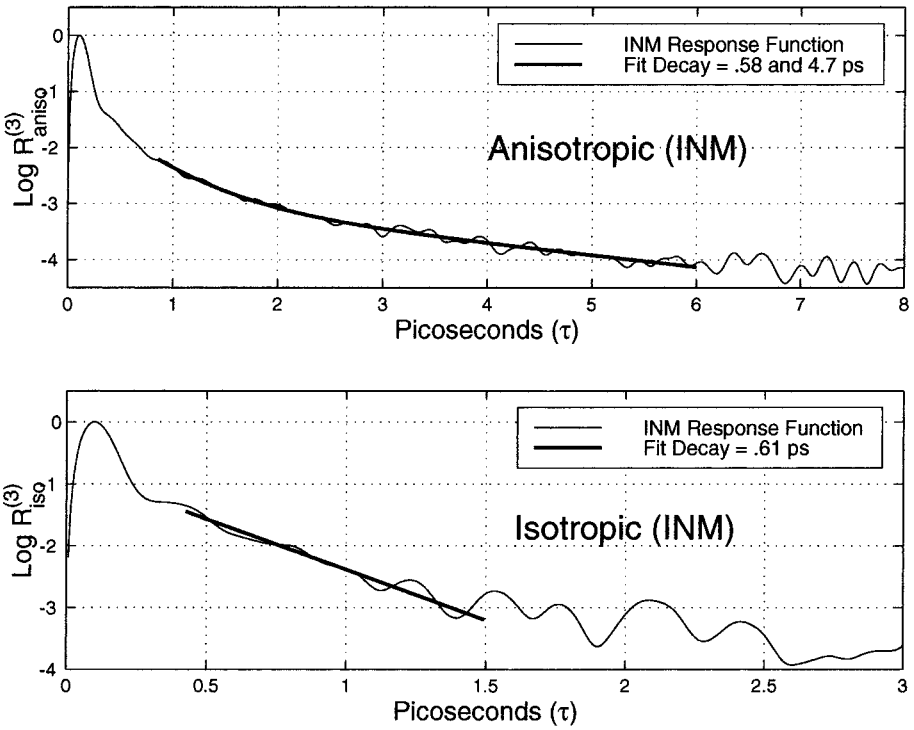

Figure 5. Anisotropic and isotropic impulse nuclear response functions of CS_2 (at 295 K) determined by instantaneous normal mode calculation. These response functions are given by the imaginary part of the Fourier transform of the polarizability-weighted optical Kerr effect density of states. Fits to a single and double exponential for the isotropic and anisotropic response functions, respectively, are also shown in this figure.

time was also reported in a recently submitted diffractive optic based OHD polarization study.[52]

Although not controversial, the longer time scale decay dominating the anisotropic response (1.6−1.7 ps) is clearly due to the orientational diffusive motion of the liquid ensemble because it dominates the decay of anisotropic response in contrast to the decay of the isotropic component.[10,44] Molecular dynamics (MD) simulations[37,53] and INM calculations[5] have shown that the anisotropic response is dominated by contributions of the molecular contributions to the total polarizability. The isotropic response, in contrast, is dominated by the effects of collision-induced scattering.[5,53] Thus, the similar decay times (∼0.5 ps) of the isotropic and anisotropic responses, apart from that due to rotational diffusion, suggests that the librational and collision-induced scattering are phenomnologically damped by the same mechanism(s). In other words, the same phenomenological damping rate is observed regardless of the coupling mechanism responsible for the Raman activity of these intermolecular modes (rotational diffusion aside). A recent MD simulation[37] determined an exponential relaxation time (in the 0.5−2.0 ps regime) of 0.62 ps for the collision-induced many body polarizability component of CS_2 is good agreement with the time scale evident here for the decay of the isotropic response.

This observed ∼0.5 ps decay, in principle, may be associated with some dynamical relaxation processes, such as lifetime decay, pure-dephasing, or spectral narrowing.[5] A time scale of approximately 400−600 fs is not an unreasonable estimate for these processes for such intermolecular modes in liquids at room temperature. Alternatively, this decay could result from the inhomogeneous distribution of Raman-coupled density of intermolecular states, as was previously proposed by McMorrow and Lotshaw.[6,8,17] Figure 5 shows the calculated isotropic and anisotropic nuclear impulse response functions given by the imaginary part of the Fourier transforms of the corresponding INM Raman-weighted spectral density. The INM calculation methods are detailed elsewhere, and the results shown here include contributions from only the real INMs.[54,55] These results are relatively insensitive to this choice. The best fits of single and double exponential decays to the INM isotropic and anisotropic response functions are also displayed in Figure 5. Mimicking the experimental results (Figure 4), a subpicosecond decay is more evident in the isotropic response and hence a single-exponential fit is shown here. It is clear that this intermediate time scale (∼0.5 ps) is present in both the isotropic and anisotropic INM calculated response functions. The INM method, as expected, does not capture the rotational reorientation dynamics, and the predicted longer time constant (∼4.7 ps) in the calculated INM anisotropic response (Figure 5) should fail as a quantitative measure of this relaxation rate. However, the INM results are in near quantitative agreement with the corresponding MD derived time correlation function results in this intermediate time and frequency regime, and the time correlation results agree extremely well with the experimental data.[54,55] The INM spectral density is just the underdamped inhomogeneous broadening limit description of such Raman response functions. This suggests that the underlying dynamics responsible for the commonly observed intermediate time scale may be a consequence of the shape of the typical polarizability-weighted density of intermolecular vibrational shapes, which is itself a sum of the characteristically shaped hindered translational and rotational contributions. These calculated results are in substantial ageement with the inhomogeneous broadening explanation argued earlier by McMorrow and Lotshaw.[8]

V. Conclusion

A relatively simple, novel method for the observation of polarization-specific impulsively excited Raman responses in transparent liquids is described here. The responses obtained by this technique demonstrate how the usually putative dichroic

responses of electronically nonresonant materials can be enhanced when only a frequency selected portion of the probe pulse is observed. These responses are obtained in the simple two-beam pump−probe configuration when only a single optical element, a band-pass filter, is added in the probe beam path. Since the dichroism is inherently an in-phase local oscillator measurement, this technique allows the observation of ultrafast responses for any relative orientation of pump and probe polarization vectors. Furthermore, a subtle, but nonetheless fundamental point regarding these *dispersed* dichroic observations is that these transients are generated by a response function that can be all real (see Figure 1). This is probably a reasonable approximation for the lowest frequency components of the Raman spectral density. Dispersed dichroic responses derived from higher frequency components of the Raman active spectral density must have contributions from both the real and imaginary parts of $R^{(3n)}_{ijkl}(t)$ since these features dominate the, albeit weak, observed integrated dichroic OHD signals of nonresonant liquids. Modeling the temperature dependence of the real and imaginary portions of the nuclear impulse response function may prove to be an additionally useful probe of the nature of these low-frequency responses.[39]

In a subsequent report we show how the spectral density corresponding to the Raman impulse response function can be obtained from the observed partially integrated dichroic responses when it is normalized by the corresponding partially integrated nonresonant electronic response (see Appendix).[56] However, we note here that the relative weighting of the different nuclear components of the third-order impulse response function are different for dichroic and birefringent measurements of the same polarizability element for equivalent pulses. Higher frequency components make relatively larger contributions to dichroic as compared to birefringent observations for the same impulse response function and pulse shape. Thus, 0.5 and 1.7 ps CS_2 decays may appear with different relative magnitudes in the dichroic and birefringent measurements of the same polarizability component. For example, the 0.5 ps decay is about 3 times as large relative to the 1.7 decay component in the experimental anisotropic response we have observed by dichroic as compared to birefringent methods.

The dichroic isotropic response of CS_2 is found to decay predominantly with a relaxation time of ~0.5 ps. This decay time closely matches the nondiffusive relaxation time of the birefringent and dichroic anisotropic responses of CS_2. Both the librational and collision-induced nuclear responses appear to be governed by the same relaxation mechanism, apart from rotational reorientational relaxation. The INM calculation results presented here support the role that the distribution of the Raman-coupled density of states, i.e., inhomogeneous broadening, plays in determining this time scale. Comparison of the anisotropic and isotropic $P^{(3)}$ response in a number of liquids (and state points), as well as the analysis of higher order Raman responses, could further help establish the nature of this decay process.

Acknowledgment. The support of the National Science Foundation (grant CHE-9712725) and the Boston University Photonics Center is gratefully acknowledged.

Appendix

The dispersed pump−probe spectrogram due to a nonresonant electronic (instantaneous) response only, i.e., $R^{(3)}(\tau) \propto \delta(\tau)$, at detected probe frequency Δ_D and interpulse delay τ is given by[40,41]

$$S_{el}(\Delta_D,\tau) = -2\mathrm{Im}[\exp(-i\theta)\int_{-\infty}^{\infty} dt_1 \exp(-i\Delta_D t_1) \times I^{pu}(t_1)\int_{-\infty}^{\infty} dt_2 \exp(i\Delta_D t_2)\, \hat{E}^{pr}(t_1-\tau)\, \hat{E}^{*pr}_{l}(t_2-\tau)] \quad \text{(A1)}$$

This expression results from eqs 1−3 when the first probe pulse interaction precedes the second pump field interaction.[41] The field polarization directions indices (*ijkl*) have been omitted for brevity and $I^{pu} = |E^{pu}|^2$.

Convolution of the total (electronic and nuclear) third-order response function with this frequency selected electronic response, $S_{el}(\Delta_D,\tau)$, yields

$$R^{(3)}(\tau) \otimes S_{el}(\Delta_D,\tau) = \int_{-\infty}^{\infty} d\tau'\, R^{(3)}(\tau')\, S_{el}(\Delta_D,\tau-\tau') \quad \text{(A2)}$$

$$= -2\mathrm{Im}[\exp(-i\theta)\int_{-\infty}^{\infty} d\tau' \int_{-\infty}^{\infty} dt_1 \exp(-i\Delta_D t_1)\, I^{pu}(t_1)\int_{-\infty}^{\infty} dt_2 \exp(i\Delta_D t_2)\, \hat{E}^{pr}(t_1-\tau+\tau')\, \hat{E}^{*pr}(t_2-\tau+\tau')\, R^{(3)}(\tau')] \quad \text{(A3)}$$

When $t = t_1 + \tau'$ and $t' = t_2 + \tau'$, the convolution can be rewritten as

$$R^{(3)}(\tau) \otimes S_{el}(\Delta_D,\tau) = -2\mathrm{Im}[\exp(-i\theta)\int_{-\infty}^{\infty} dt \exp(-i\Delta_D t) \times \hat{E}^{pr}(t-\tau)\int_{-\infty}^{\infty} dt' \exp(i\Delta_D t')\, \hat{E}^{*pr}(t'-\tau)\int_{-\infty}^{\infty} d\tau'\, R^{(3)}(\tau') \times I^{pu}(t-\tau')] = S(\Delta_D,\tau) \quad \text{(A4)}$$

The last equality is the expression that results when eqs 2 and 3 are substituted in eq 1. Thus, by the convolution theorem, the normalized spectral density due to the third-order response function is given by the quotient of the Fourier-transformed frequency-selected experimental response and that due to the corresponding electronic-only response.

$$R^{(3)}(\omega) = \mathcal{F}\{R^{(3)}(\tau)\} = \frac{\mathcal{F}\{S(\Delta_D,\tau)\}}{\mathcal{F}\{S_{el}(\Delta_D,\tau)\}} \quad \text{(A5)}$$

A frequency-selected electronic only response may be obtained by replacing the sample with a material that has a response dominated by electronic contributions (such as quartz).

References and Notes

(1) Herzberg, G. *Infrared and Raman Spectra*; Van Nostrand: Princeton, NJ, 1945.
(2) McClain, W. M.; Harris, R. A. *Excited States*; Lim, E. C., Ed.; Excited States, Vol. 3; Academic: New York, 1977; p 1.
(3) Berne, B. J.; Pecora, R. *Dynamic Light Scattering*; John Wiley &Sons: New York, 1976.
(4) Frenkel, D.; McTague, J. P. *J. Chem. Phys.* **1980**, *72*, 2801.
(5) Murry, R. L.; Fourkas, J. T.; Keyes, T. *J. Chem. Phys.* **1998**, *109*, 2814.
(6) Kalpouzos, C.; McMorrow, D.; Lotshaw, W. T.; Kenney-Wallace, G. A. *Chem. Phys. Lett.* **1988**, *150*, 138.
(7) McMorrow, D.; Lotshaw, W. T. *Chem. Phys. Lett.* **1990**, *174*, 85.
(8) McMorrow, D.; Lotshaw, W. T. *Chem. Phys. Lett.* **1991**, *178*, 69.
(9) McMorrow, D.; Lotshaw, W. T. *J. Phys. Chem.* **1991**, *95*, 10395.
(10) Cho, M.; Du, M.; Scherer, N. F.; Fleming, G. R.; Mukamel, S. *J. Chem. Phys.* **1993**, *99*, 2410.
(11) Castner, E. W., Jr.; Chang, Y. J. *J. Chem. Phys.* **1993**, *99*, 113, 7289.
(12) Ziegler, L. D.; Fan, R.; Desrosiers, A. E.; Scherer, N. F. *J. Chem. Phys.* **1994**, *100*, 1823.
(13) Duel, H. P.; Cong, P.; Simon, J. P. *J. Phys. Chem.* **1994**, *98*, 12600.
(14) Chang, Y. J.; Castner, E. W. *J. Phys. Chem.* **1994**, *98*, 9712; **1996**, *100*, 3330.
(15) Lotshaw, W. T.; McMorrow, D.; Thantu, N.; Melinger, J. S.; Kitchenham, R. *J. Raman Spectrosc.* **1995**, *26*, 5571.
(16) Palese, S.; Mukamel, S.; Miller, R. J. D.; Lotshaw, W. T. *J. Phys. Chem.* **1996**, *100*, 10380.
(17) McMorrow, D.; Thantu, N.; Melinger, J. S.; Kim, S. K.; Lotshaw, W. T. *J. Phys. Chem.* **1996**, *100*, 10389.

(18) Farrer, R. A.; Loughnane, B. J.; Deschenes, L. A.; Fourkas, J. T. *J. Chem. Phys*. **1997**, 106.
(19) Steffen, T.; Meinders, N. A. C. M.; Duppen, K. *J. Phys. Chem. A* **1998**, *102*, 4213.
(20) Bartolini, P.; Ricci, M.; Torre, R.; Righini, R.; Santa, I. *J. Chem. Phys*. **1999**, *110*, 8653.
(21) Eesly, G. L.; Levenson, M. D.; Tolles, W. M. *IEEE J. Quantum Electron*. **1978**, *14*, 45. Levenson, M. D.; Eesley, G. L. *Appl. Phys. Lett*. **1979**, *19*, 1.
(22) Vohringer, P.; Scherer, N. F. *J. Phys. Chem*. **1995**, *99*, 2684.
(23) Cong, P.; Chang, Y. J.; Simon, J. D. *J. Phys. Chem*. **1996**, *100*, 8613.
(24) Chang, Y. J.; Cong, P.; Simon, J. D. *J. Chem. Phys*. **1997**, *106*, 8639.
(25) Matsuo, S.; Tahara, T. *Chem. Phys. Lett*. **1997**, *264*, 636.
(26) Khalil, M.; Demirdoven, N.; Golonzka, O.; Fecko, C. J.; Tokmakoff, A. *J. Phys. Chem. A* **2000**, *104*, 5711.
(27) Khalil, M.; Golonzka, O.; Demirdoven, N.; Fecko, C. J.; Tokmakoff, A. *Chem. Phys. Lett*. **2000**, *321*, 231.
(28) Gardecki, J. A.; Yu, G.; Constantine, S.; Peng, J.; Zhou, Y.; Ziegler, L. D. *J. Chem. Phys*. **2001**, *114*, 3586.
(29) Sheik-Bahae, M.; Said, A. A.; Van Stryland, E. W. *Opt. Lett*. **1992**, *17*, 258.
(30) Sheik-Bahae, M.; Said, A. A.; Wei, T.-H.; Hagan, D. J.; Van Stryland, E. W. *IEEE J. Quantum Electron*. **1990**, *26*, 760.
(31) Kawazoe, T.; Kawaguchi, H.; Inoue, J.; Haba, O.; Ueda, M. *Opt. Commun*. **1999**, *160*, 125.
(32) Geiger, L. C.; Ladanyi, B. M. *J. Chem. Phys*. **1987**, *87*, 199.
(33) Chang, Y. J.; Cong, P.; Simon, J. D. *J. Phys. Chem*. **1995**, *99*, 7857.
(34) Goodno, G.; Dadusc, G.; Miller, R. J. D. *J. Opt. Soc. Am. B* **1998**, *15*, 1791.
(35) Keyes, T. *J. Chem. Phys*. **1996**, *104*, 9349.
(36) Tokmakoff, A.; Fleming, G. R. *J. Chem. Phys*. **1997**, *106*, 2569.
(37) Kiyohara, K.; Kamada, K.; Ohta, K. *J. Chem. Phys*. **2000**, *112*, 6338.
(38) Loughnane, B. J.; Scodinu, A.; Farrer, R. A.; Fourkas, J. T. *J. Chem. Phys*. **1999**, *111*, 2686.
(39) Mukamel, S. *Nonlinear Optical spectroscopy*; Oxford University Press: Oxford, U.K., 1995.
(40) Gardecki, J. A.; Constantine, S.; Zhou, Y.; Ziegler, L. D. *J. Opt. Soc. Am. B* **2000**, *17*, 652.
(41) Zhou, Y.; Constantine, S.; Gardecki, J. A.; Ziegler, L. D. *Chem. Phys. Lett*. **1999**, *314*, 73.
(42) McMorrow, D.; Lotshaw, W. T.; Kenney-Wallace, G. A. *IEEE J. Quantum Electron*. **1988**, *24*, 443.
(43) Constantine, S.; Zhou, Y.; Morais, J.; Ziegler, L. D. *J. Phys. Chem. A* **1997**, *101*, 5456.
(44) Cho, M.; Fleming, G. R.; Mukamel, S. *J. Chem. Phys*. **1993**, *98*, 5314.
(45) Zhou, Y.; Constantine, S.; Harrel, S.; Ziegler, L. D. *J. Chem. Phys*. **1999**, *110*, 5893.
(46) Levenson, M. D.; Kano, S. S. *Introduction to Nonlinear Laser Spectrocopy*; Academic Press: New York, 1988.
(47) Tokmakoff, A. *J. Chem. Phys*. **1996**, *105*, 1.
(48) Hellwarth, R. W. *Prog. Quantum Electron*. **1977**, *5*, 1.
(49) Frenkel, D.; McTague, J. P. *J. Chem. Phys*. **1980**, *72*, 2801.
(50) Tokmakoff, A. Private communication.
(51) Keyes, T.; Ladanyi, B. Private communication.
(52) Xu, Q.-H.; Ma, Y.-Z.; Fleming, G. R. *Chem. Phys. Lett*. **2001**, *338*, 254.
(53) Geiger, L. C.; Ladanyi, B. M. *J. Chem. Phys*. **1989**, *89*, 6588.
(54) Ji, X.; Ahlborn, H.; Moore, P.; Space, B. *J. Chem. Phys*. **2000**, *113*, 8693.
(55) Ji, X.; Ahlborn, H.; Moore, P.; Zhou, Y.; Constantine, S.; Ziegler, L. D.; Space, B. *J. Chem. Phys*. **2000**, *112*, 4186.
(56) Ziegler, L. D.; Gardecki, J. A.; Constantine, S.; Zhou, Y. Manuscript in preparation.